Journal of Hydrology 557 (2018) 910–915

Contents lists available at ScienceDirect

Journal of Hydrology

journal homepage: www.elsevier.com/locate/jhydrol

Technical Note

Effects of horizontal grid resolution on evapotranspiration partitioning using TerrSysMP

P. Shrestha [a,*], M. Sulis [b], C. Simmer [a,d], S. Kollet [c,d]

[a] Meteorological Institute, University of Bonn, Germany
[b] Luxembourg Institute of Science and Technology (LIST), Environmental Research and Innovation, Luxembourg
[c] Institute for Bio- and Geosciences, Agrosphere (IBG-3) Research Centre Juelich, Germany
[d] Centre for High-Performance Scientific Computing in Terrestrial Systems (HPSC TerrSys) Geoverbund ABC/J, Germany

ARTICLE INFO

Article history:
Received 30 May 2017
Received in revised form 15 December 2017
Accepted 9 January 2018
Available online 10 January 2018
This manuscript was handled by Tim R. McVicar, Editor-in-Chief, with the assistance of Yongqiang Zhang, Associate Editor

Keywords:
Integrated surface-groundwater flow modeling
Terrestrial Systems Modeling Platform
Model grid resolution
Uncertainty in T/ET estimates

ABSTRACT

Biotic leaf transpiration (T) and abiotic evaporation (E) are the two major pathways by which water is transferred from land surfaces to the atmosphere. Earth system models simulating the terrestrial water, carbon and energy cycle are required to reliably embed the role of soil and vegetation processes in order to realistically reproduce both fluxes including their relative contributions to total evapotranspiration (ET). Earth system models are also being used with increasing spatial resolutions to better simulate the effects of surface heterogeneity on the regional water and energy cycle and to realistically include effects of subsurface lateral flow paths, which are expected to feed back on the exchange fluxes and their partitioning in the model.

Using the hydrological component of the Terrestrial Systems Modeling Platform (TerrSysMP), we examine the uncertainty in the estimates of T/ET ratio due to horizontal model grid resolution for a dry and wet year in the Inde catchment (western Germany). The aggregation of topography results in smoothing of slope magnitudes and the filtering of small-scale convergence and divergence zones, which directly impacts the surface-subsurface flow. Coarsening of the grid resolution from 120 m to 960 m increased the available soil moisture for ground evaporation, and decreased T/ET ratio by about 5% and 8% for dry and wet year respectively. The change in T/ET ratio was more pronounced for agricultural crops compared to forested areas, indicating a strong local control of vegetation on the ground evaporation, affecting the domain average statistics.

1. Introduction

Terrestrial evapotranspiration (ET) follows two pathways of soil water vaporization: 1) abiotic water evaporation (E) from the soil pores, and also surfaces of leaves, and plant residues, and 2) biotic leaf transpiration (T) via stomata exchange (Katul et al., 2012). Many studies estimate these flow pathways of water and their relative contributions to the total exchange at continental and global scales using modeling (e.g. Lawrence et al., 2007; Choudhury and DiGirolamo, 1998; Dirmeyer et al., 2006; Miralles et al., 2011; Maxwell and Condon, 2016; Zhang et al., 2016; Fatichi and Pappas, 2017) and measurements based on isotope-based methods (e.g.Schlesinger and Jasechko, 2014; Jasechko et al., 2014; Coenders-Gerrits et al., 2014; Evaristo et al., 2015; Good et al., 2015).

Maxwell and Condon (2016) show with a continental-scale integrated hydrology model at a horizontal grid resolution of 1 km that the inclusion of surface and groundwater lateral flow increased the domain averaged T/ET ratio from $47 \pm 13\%$ to $62 \pm 12\%$, which better agrees with estimates from recent isotope-based methods. At continental scales, the attainable horizontal grid resolution is mainly limited by the available computational resources to achieve horizontal grid resolutions on the order of 1–10 km and the availability of high-resolution atmospheric forcing data (>10 km) including soil and landuse data. However, at these grid resolutions without additional subgrid parameterizations, the simulated surface energy flux partitioning may depend on the grid resolution itself. Coarsening of the grid resolution smoothens the local slopes and removes small-scale soil water convergence and divergences zones along simulated river corridors and water divides, and impacts the soil moisture distribution

* Corresponding author at: Meckenheimer Allee 176, Meteorological Institute, University of Bonn, Germany.
E-mail address: pshrestha@uni-bonn.de (P. Shrestha).

https://doi.org/10.1016/j.jhydrol.2018.01.024
0022-1694/

leading to an effectively reduced drainage (Zhang and Montgomery, 1994; Kuo et al., 1999; Sulis et al., 2011; Shrestha et al., 2014; Shrestha et al., 2015 of many others). For example, using an integrated hydrology model for the Inde catchment (325 km^2) in western Germany, Shrestha et al. (2015) showed that the simulated exchange processes strongly depend on the horizontal grid resolution due to changes in the non-local controls of soil moisture. In this study, we build upon their results and examine the impact of the horizontal grid resolution on the model simulated water fluxes with a particular emphasis on the uncertainty of T/ET model estimates, for a relatively wet and relatively dry year.

The rest of the manuscript is organized as follows: Sections 2 and 3 describes the model and the experiment design for this study. Results and discussions are presented in Sections 4 and 5 respectively. Finally, conclusions are presented in Section 6.

2. Model description

The hydrological component of the Terrestrial Systems Modeling Platform (TerrSysMP; Shrestha et al., 2014, 2015) consists of the NCAR community Land Model CLM3.5 (Oleson et al., 2008) and the 3D variably saturated groundwater and surface water flow model ParFlow (Kollet and Maxwell, 2006, Maxwell, 2013). A detailed description of the coupling between the models can be found in Shrestha et al. (2014) and Shrestha et al. (2015). Here, we briefly discuss the relevant parameterization in the land surface model, which controls the pathways of evapotranspiration.

In CLM3.5, the surface heterogeneity of a grid cell is represented using a subgrid tile approach at different hierarchy levels with five landunits, multiple soil columns, and 17 plant functional types (PFTs), which also includes the bare soil (i.e., without vegetation). An explicit canopy layer represents the PFTs and a lookup table provides the PFT specific photosynthetic, optical, aerodynamic, and vertical root distribution parameters. While a grid cell can include multiple PFTs (e.g., 80% crop and 20% bare soil), in this study, we use one soil column and one PFT in each grid cell. Solar radiation absorbed by the canopy and the ground below is computed via radiative transfer within vegetative canopies, which depends on the incoming solar radiation, LAI, and optical properties of the PFT; the latter remain constant in time. ET from a vegetated surface is computed as the sum of water vapor flux due to canopy evaporation from wet leaf surfaces, transpiration from dry leaf surfaces and evaporation from ground below. The stomatal resistance for computing canopy transpiration is coupled to photosynthesis based on the models of Farquhar et al. (1980) and Collatz et al. (1991). Leaf photosynthesis is a prognostic variable and depends on the maximum rate of carboxylation, which again depends on PFT specific photosynthetic parameters including leaf temperature and is downregulated for nitrogen limitation and root zone soil moisture limitation.

For vegetated surface, ground evaporation depends on the aerodynamic resistance and the humidity gradient between ground and canopy. Soil surface specific humidity is computed by scaling the saturation specific humidity at soil temperature, with a factor $\propto$, which is a weighted combination of values for snow and soil. The $\propto_{soil}$ is a function of surface soil water matric potential and ground temperature. Excessive soil evaporation for no snow conditions is reduced by an additional soil resistance term, which depends on the relative saturation of the top layer, and decreases exponentially with the increase in relative saturation.

3. Experiment design

TerrSysMP was set up over the Inde catchment (325 km^2) encompassing the Wehebach tributary (~50 m amsl) and drains the northern foothills of the lower Eifel mountain range (~600 m amsl) in western Germany. This model setup is consistent with the one used in Shrestha et al. (2015). Land use in the region based on CLM3.5 plant functional types (PFTs) changes from mostly agricultural crops (c1n) near the foothills to needle-leaf evergreen trees (nle) and broadleaf deciduous trees (bld) along the northern slopes of Eifel mountain range. The urban land cover in the catchment (~17% of catchment area) is represented as agricultural canopy (c1f) with a fixed leaf area index (LAI = 0.6), as the urban module is absent in CLM3.5. This is not meant to represent the actual physical processes over the urban area but the use of fixed low LAI reduces the local control of vegetation in these areas, when investigating the impact of grid resolution on simulated physical processes. A uniform soil texture is used, which largely follows the information found in BK50 1:50,000 scale data (http://www.gd.nrw.de/pr_shop_informationssysteme_bk50d.htm). By using a complete homogeneous soil texture, we also remove any effects of scaling of soil hydraulic properties. The available 15 m landuse data (Waldhoff, 2012) and 90 m Shuttle Radar Topography Mission (SRTM) topography data were aggregated to 120, 240, 480 and 960 m horizontal grid resolution by assigning each grid cell with its dominant PFT according to the high resolution data. With successive grid coarsening when aggregating topography, the skewness of the distribution of plan curvature changes from −0.07 to −99.43, while its kurtosis varies from 3.64 to 13273.9. Similarly, for the profile curvature, skewness and kurtosis change from approximately 0.24 to −0.92 and 0.59 to 5.66, respectively.

In this study, a wet and a dry year were chosen with average accumulated annual precipitation of 1002 *mm* (*Year* 2009) and 695 *mm* (*Year* 2011) respectively for the catchment. Based on seven year COSMO-DE forcing data (2007–2015), 2011 has the minimum annual precipitation, whereas the annual precipitation for 2009 is closer to the median value. Similar as the year 2009, 2010 was also wet year relative to 2011, with an annual rainfall of 944 mm. The model was spunup over a 6-year period for the different spatial resolutions using the same annual atmospheric forcing data (COSMO-DE analysis with 2.8 km resolution). The spin-up for 2009 and 2011 was done separately, using the same hydrostatic profile with groundwater table depth at 5 m below the land surface for soil moisture initialization. This approach was chosen to generate consistent initial conditions dependent only on the simulated year. The temporal evolution of total unsaturated storage approaches a quasi-equilibrium state in the fifth year (see Shrestha et al., 2015 for details). The output for the sixth year (2009 or 2011) is analyzed with respect to the groundwater table (GWT) depth and the pathways of water fluxes for evaporation and transpiration during the months of April to September, with higher incoming solar radiation. For our analysis the coarser grid resolution output was disaggregated to the highest resolution by attributing to each high resolution 120 m × 120 m grid cell the same value of the coarser grid cell to which it belonged.

4. Results

Coarsening of the grid resolution shifts the frequency distribution of GWT depth for both years towards shallower depths (Fig. 1). The modeled domain and time averaged GWT depth and standard deviation for April to September for 2009 were $3.55 \pm 4.60m$, $1.88 \pm 2.96m$, $0.56 \pm 1.26m$, $0.16 \pm 0.28m$ for the grid resolutions 120 m, 240 m, 480 m and 960 m respectively. For 2011, the values were $5.43 \pm 5.58m$, $3.60 \pm 4.33m$, $1.85 \pm 2.72m$, $0.78 \pm 1.32m$ respectively. At 120 m grid resolution, the GWT depth distribution is similar for both years with only a slightly higher frequency of zones with shallow GWT depth (<0.2 m) for the wetter year. The shift towards higher frequencies of shallower

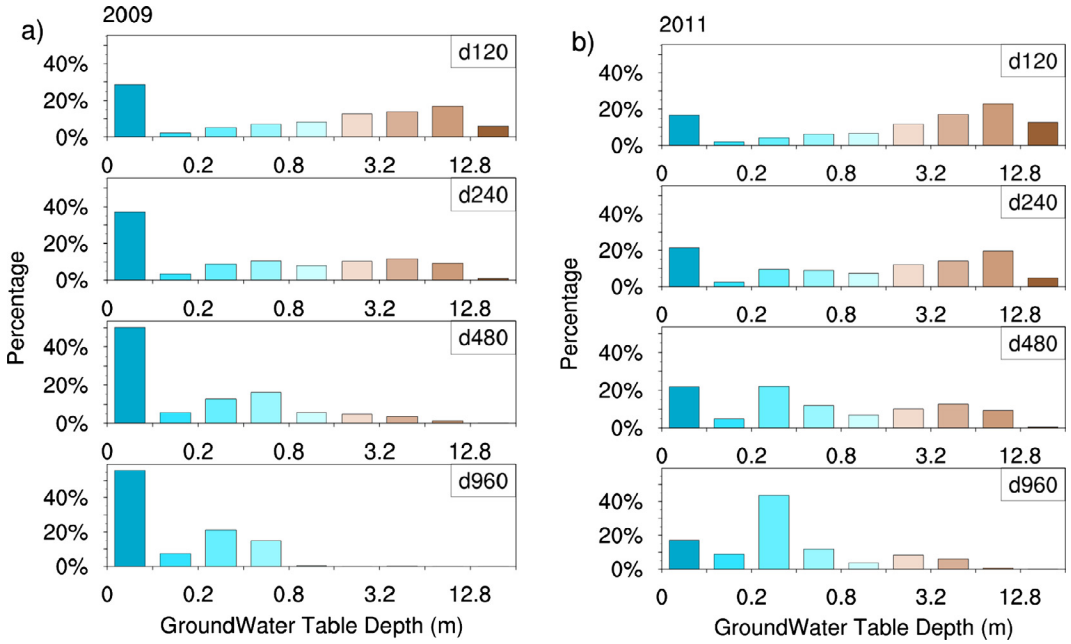

Fig. 1. Frequency Distribution of Groundwater Table Depth from April to September for River Inde. The top left corner of each subplot represents the domain grid resolution in meters.

GWT depths with grid coarsening depends on the overall soil moisture and thus annual precipitation. For the wetter year, the zones with shallow GWT depth (<0.2 m) increase substantially with grid coarsening at the expense of regions with deeper GWT depths, while for the drier year the shift from deep GWT depths results in substantial increase in zones with GWT depth from 0.2 to 0.8 m.

We now examine the dependence of E and T, and T/ET on the horizontal grid resolution. Fig. 2a shows the spatial PFT distribution with GWT depths deeper than 1.6 m during mid June for 2009 and 2011, which remains similar throughout the year. This threshold of 1.6 m is applied to mask the regions with shallow GWT, as observed in the frequency distribution of coarsest model runs for both years (see Fig. 1). Zones with deeper GWT depth are mostly found along the hillslopes, while the masked-out shallow GWT regions stretch along the streams and the flat area near the Inde outlet. The mask for the wet year (2009) has slightly smaller coverage compared to the dry year (2011).

Mean and standard deviation of the solar radiation absorbed by vegetation and ground do not change much with grid coarsening. The sum of solar radiation absorbed by ground (S_{abg}) and vegetation (S_{abv}) is similar for both crop PFTs with the tree PFTs absorbing more (27 Wm^{-2} for nle and 16 Wm^{-2} for bld from April to September for both years). However, the partitioning of the solar radiation (S_{abg}/S_{abv}) is strongly controlled by the LAI and the optical parameters of the PFTs and thus differ substantially. The crops exhibit higher ratios of S_{abg}/S_{abv} compared to trees, with highest magnitude for c1f due to the fixed low LAI value. Grid coarsening, however, has no significant effect on the absorbed solar radiation and its partitioning to vegetation and ground.

Grid resolution effects are paramount for the state of the soil and its effect on the turbulent fluxes. The domain-averaged top 10 cm relative soil moisture ($\bar{S_w}$) for all PFTs increases with the grid coarsening while its variance decreases (Fig. 3). In the wet year (2009), $\bar{S_w}$ increases from 0.55 to 0.90 for forested areas (e.g., bld) and from 0.54 to 0.88 for agricultural areas (e.g., c1n). During the dry year (2011), $\bar{S_w}$ changes from 0.46 to 0.67 and from 0.46 to 0.70 for forested (bld) and agricultural (c1n) areas, respectively. For both years, the domain-averaged plant transpiration for different

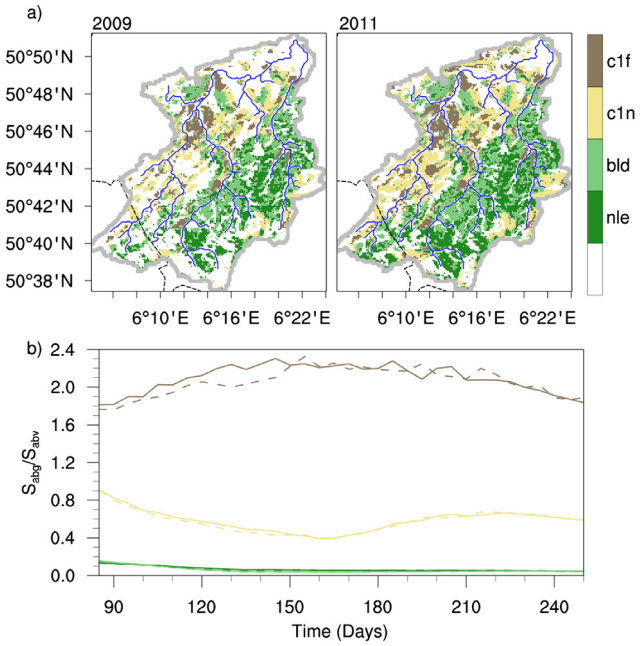

Fig. 2. a) PFT distribution for areas with modeled groundwater tables (GWTs) deeper than 1.6 m for the Inde catchment. Areas with shallower GWTs (<1.6 m) depths are masked out and left white. The codes indicate the PFTs agricultural crops (c1f), agricultural crops with constant low LAI as substitute for urban areas (c1n), broadleaf deciduous tree (bld), and evergreen needle-leaf trees (nle). Streams and catchment delineation are derived from the SRTM topography at 120 m resolution. The dashed line indicates the frontier between Germany and Belgium. b) Time series of the spatially (over the catchment) and temporally averaged (over 5 days) partitioning of absorbed solar radiation (S_{abg}/S_{abv}) for 2009 (solid lines) and 2011 (dotted lines). The colors for different PFTs are consistent with indices for spatial map. (For interpretation of the references to colour in this figure legend, the reader is referred to the web version of this article.)

PFTs ($\bar{T}$) does not change much with the increase in soil moisture due to grid coarsening, while evaporation ($\bar{E}$) does (Fig. 3). This effect is stronger for PFTs with low LAI due to the higher amounts

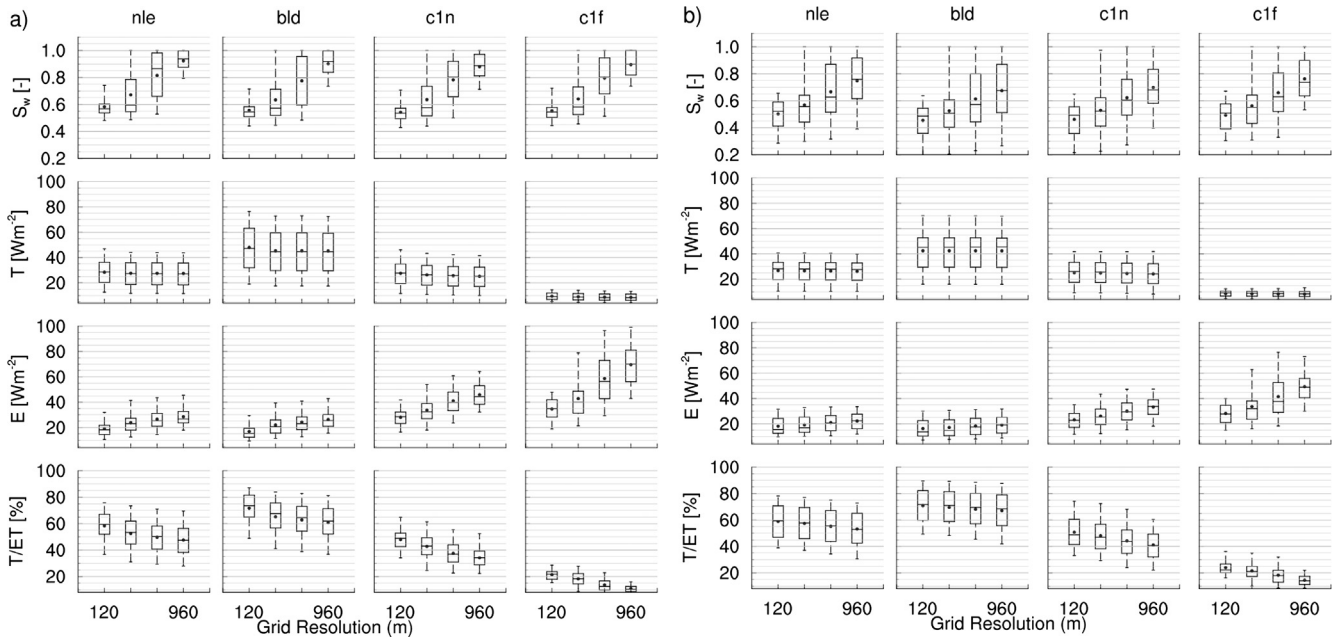

Fig. 3. Scaling behavior of relative soil moisture (S_w), canopy transpiration (T), evaporation (E) and the ratio of transpiration to total evapotranspiration (T/ET) with grid resolution for a) wet year (2009) and b) dry year (2011). The codes indicate the PFTs agricultural crops (c1f), agricultural crops with constant low LAI as substitute for urban areas (c1n), broadleaf deciduous tree (bld), and evergreen needle-leaf trees (nle). The box plot and the whiskers show the mean (solid markers), median, 5, 25, 75 and 95th percentile.

of solar radiation absorbed by the ground (see Fig. 2b) and higher available soil moisture for ground evaporation (Fig. 3a and b). The bare soil evaporation parameterization, which depends on the available soil moisture on the top layer, dominates this behavior. Accordingly, total evapotranspiration increases with grid coarsening and thereby decreases the domain average $T/\bar{ET}$ for all PFTs (Fig. 3a and b). This decrease is relatively higher for the wet year than for the dry year.

The magnitudes of the variation of $\bar{E}$ and $T/\bar{ET}$ ratio in terms of mean and one standard deviation are presented in Table 1 and 2. $\bar{E}$ is higher for the 2009 compared to 2011 because of the higher available soil moisture. Vegetation cover strongly controls the local ground evaporation depending on the PFT optical parameters and the leaf area index (LAI). With their higher transmissivity for incoming radiation, the variation in ground evaporation is higher for crops compared to forest and even higher for crops with low LAI.

At 120 m grid resolution, the $T/\bar{ET}$ is similar in both years for all PFTs: 58–59% for needle leaf evergreen trees, 71–72% for broadleaf deciduous trees, 48–51% for agricultural crop and 21–24% for crop with fixed low LAI. With grid coarsening from 120 to 960 m, the $T/\bar{ET}$ decreases by different magnitudes between the wet and dry year for different PFTs (see Table 2). For the wet year, $T/\bar{ET}$ decreases between 10–14% for crops and 10–11% for trees; for the dry year, its decrease is around 10% for the crops and 4–6% for trees. In terms of domain average, including all PFTs, the $T/\bar{ET}$ decreases with grid coarsening by around 5% and 8% for the dry and wet year, respectively.

5. Discussions

This study addresses the grid-resolution dependence of $T/\bar{ET}$ simulated by physically-based models, which include surface and 3D subsurface lateral flow. Grid coarsening decreases the mean and variance of GWT depth, an effect more amplified during the wet year. The induced increase in near surface soil moisture increases the ground evaporation while transpiration remained almost constant. Accordingly, in the central European mid-latitude climate regime root zone soil moisture is usually not the limiting factor for transpiration. Thus with respect to transpiration the system is energy limited. Modeled ground evaporation mainly depends on the upper layer soil moisture and increases with moister soil suggesting a water limited state. According to the study by Maxwell and Condon (2016) the inclusion of surface and groundwater lateral flow increases the domain averaged $T/\bar{ET}$ for the continental US by almost 15%. In a more recent study,

Table 1
Domain averaged evaporation (E [Wm^{-2}]) from April to September for different PFTs. The codes indicate the PFTs agricultural crops (c1f), agricultural crops with constant low LAI as substitute for urban areas (c1n), broadleaf deciduous tree (bld), and evergreen needle-leaf trees (nle). Also provided are the numbers of grid cells of each PFT in the catchment at their native grid resolution.

PFT	120 m 2009/2011	240 m 2009/2011	480 m 2009/2011	960 m 2009/2011
nle	19 ± 7/18 ± 7	24 ± 9/19 ± 7	27 ± 9/21 ± 7	28 ± 8/22 ± 7
#	5390	1376	382	92
bld	17 ± 7/16 ± 7	22 ± 8/17 ± 8	24 ± 9/18 ± 8	26 ± 8/19 ± 7
#	5899	1419	353	80
c1n	28 ± 7/23 ± 7	34 ± 10/26 ± 9	41 ± 11/30 ± 10	46 ± 10/33 ± 9
#	7187	1815	508	106
c1f	35 ± 9/28 ± 9	43 ± 18/34 ± 15	59 ± 21/41 ± 17	70 ± 17/49 ± 13
#	4018	1015	257	58

Table 2
Domain averaged ratio of transpiration to total evapotranspiration (T/ET [%]) from April to September for different PFTs. The codes indicate the PFTs agricultural crops (c1f), agricultural crops with constant low LAI as substitute for urban areas (c1n), broadleaf deciduous tree (bld), and evergreen needle-leaf trees (nle).

PFT	120 m 2009/2011	240 m 2009/2011	480 m 2009/2011	960 m 2009/2011
nle	58 ± 12/59 ± 13	53 ± 13/57 ± 13	50 ± 13/55 ± 14	48 ± 12/53 ± 13
bld	72 ± 12/71 ± 13	65 ± 14/70 ± 14	63 ± 14/68 ± 14	61 ± 14/67 ± 14
c1n	48 ± 9/51 ± 12	43 ± 10/48 ± 13	38 ± 10/44 ± 13	34 ± 9/41 ± 12
c1f	21 ± 4/24 ± 6	18 ± 5/22 ± 7	14 ± 5/18 ± 7	11 ± 3/14 ± 4

using a modified Budyko framework, Freund and Kirchner (2017) also illustrate variable biases on estimated ET depending on hypothetical transfer of water due to gravity between regions of different altitudes and aridity, showing the complexity of including lateral flow. Our work suggests that for wet regimes, the increased grid resolution might increase T/ET ratios as found in Maxwell and Condon (2016) due to non-local control on soil moisture, which however is overall lower than the effect of including lateral flow itself, due to the strong local control of vegetation. The increase in T/ET ratios was even lower for the dry year compared to the wet year. We also investigated the impact of the initial condition on T/ET ratio for the dry year (to account for the antecedent conditions), by conducting a 6-year model spin-up for 2009 and then running the model from Jan 2009 to Dec 2011. For this approach, the domain average soil moistures for 2011 compared to the earlier approach (values in brackets) were 0.64 (0.60), 0.69 (0.64), 0.75 (0.69) and 0.77(0.74) for 120 m, 240 m, 480 m and 960 m respectively. Although the soil moisture is higher for all grid resolutions with the new runs, as expected, the changes in mean soil moisture and T/ET with grid coarsening remains similar between the two approaches. Besides, the uncertainty in T/ET due to horizontal grid resolution will also depend on the distribution of land surface heterogeneity in the domain, where vegetation type and LAI was found to exert strong control.

Additional uncertainties in T/ET do arise from photosynthetic parameters of simulated vegetation (e.g., Sulis et al., 2015), root water uptake parameterizations (e.g., Zeng et al., 1998; Feddes et al., 2001; Li et al., 2013; Wang et al., 2016; Fu et al., 2016; Ferguson et al., 2016), canopy radiative transfer controlling solar radiation absorbed by the ground (e.g., Bonan et al., 2014) and bare soil evaporation parameterizations (e.g., Sellers et al., 1996; Lawrence et al., 2012; Tang and Riley, 2013; Jefferson and Maxwell, 2015). Example, Sulis et al. (2015) showed that the inclusion of crop specific photosynthetic parameters from measurements improved the surface energy flux partitioning for energy limited system. Similar improvements were also shown by Li et al. (2013) with modified root water uptake function for arid ecosystems. While, the tuning of the parameters based on single column simulations are important for predictions, their affect on T/ET estimates for regional domains with the inclusion of lateral flow needs further investigations.

6. Conclusions

Using TerrSysMP, horizontal grid coarsening from 120 m to 960 m for the Inde catchment, was found to decrease the simulated domain-averaged $T/\bar{ET}$ by almost 5–8% due to the increased soil evaporation caused by the increase in near surface soil moisture. This sensitivity primarily arises from the aggregation of topography at coarser resolution, which smoothens spatial topographic features for efficiently redistributing the surface and groundwater. The modeled $T/\bar{ET}$ does however, depend on the energy and water limited sates of modeled transpiration and ground evaporation, respectively, as found for the Inde catchment which can be seen as representative for mid-latitude central to western European catchments. Additionally, the distribution of vegetation type and the LAI did affect the dependence of $T/\bar{ET}$ on model grid resolution.

Acknowledgements

The study was conducted with support from SFB/TR32 (www.tr32.de) "Patterns in Soil-Vegetation-Atmosphere Systems: Monitoring, Modeling, and Data-Assimilation" funded by the Deutsche Forschungsgemeinschaft (DFG). We also gratefully acknowledge the computing time (project HBN33) granted by the John von Neumann Institute for Computing (NIC) and provided on the supercomputer JURECA at Juelich Supercomputing Centre (JSC). Finally, we would like to thank the JoH editorial team and the four reviewers: Stephen Good, Brecht Martens, Laura Condon and Reed Maxwell for their valuable comments, which has helped tremendously to improve the quality of the manuscript.

References

Bonan, G.B., Williams, M., Fisher, R.A., Oleson, K.W., 2014. Modeling stomatal conductance in the earth system: linking leaf water-use efficiency and water transport along the soil–plant–atmosphere continuum. Geosci. Model Dev. 7 (5), 2193–2222.

Choudhury, B.J., DiGirolamo, N.E., 1998. A biophysical process-based estimate of global land surface evaporation using satellite and ancillary data: I. Model description and comparison with observations. J. Hydrol. 205, 164–185.

Coenders-Gerrits, A.M., Van der Ent, R.J., Bogaard, T.A., Wang-Erlandsson, L., Hrachowitz, M., Savenije, H.H., 2014. Uncertainties in transpiration estimates. Nature 506 (7487).

Collatz, G., Ball, J.T., Grivet, C., Berry, J.A., 1991. Physiological and environmental regulation of stomatal conductance, photosynthesis and transpiration: a model that includes a laminar boundary layer. Agric. For. Meterol. 54, 107–136.

Dirmeyer, P.A., Gao, X., Zhao, M., Guo, Z., Oki, T., Hanasaki, N., 2006. GSWP-2: multimodel analysis and implications for our perception of the land surface. Bull. Am. Meteorol. Soc. 87 (10), 1381–1397.

Evaristo, J., Jasechko, S., McDonnell, J.J., 2015. Global separation of plant transpiration from groundwater and streamflow. Nature. https://doi.org/10.1038/nature14983.

Farquhar, G.V., von Caemmerer, S.V., Berry, J.A., 1980. A biochemical model of photosynthetic CO_2 assimilation in leaves of C3 species. Planta 149 (1), 78–90.

Fatichi, S., Pappas, C., 2017. Constrained variability of modeled *T:ET* ratio across biomes. Geophys. Res. Lett. 44, 6795–6803. https://doi.org/10.1002/2017GL074041.

Feddes, R.A., Hoff, H., Bruen, M., Dawson, T., de Rosnay, P., Dirmeyer, P., Jackson, R.B., Kabat, P., Kleidon, A., Lilly, A., Pitman, A.J., 2001. Modeling root water uptake in hydrological and climate models. Bull. Am. Meteorol. Soc. 82 (12), 2797–2809.

Ferguson, I.M., Jefferson, J.L., Maxwell, R.M., Kollet, S.J., 2016. Effects of root water uptake formulation on simulated water and energy budgets at local and basin scales. Environ. Earth Sci. 75 (4), 316.

Fu, C., Wang, G., Goulden, M.L., Scott, R.L., Bible, K., Cardon, Z.G., 2016. Combined measurement and modeling of the hydrological impact of hydraulic redistribution using CLM4.5 at eight AmeriFlux sites. Hydrol. Earth Syst. Sci. 20, 2001–2018.

Freund, R.E., Kirchner, J.W., Budyko, A., 2017. framework for estimating how spatial heterogeneity and lateral moisture redistribution affect average evapotranspiration rates as seen from the atmosphere. Hydrol. Earth Syst. Sci. 21, 217–233. https://doi.org/10.5194/hess-21-217-2017.

Good, S.P., Noone, D., Bowen, G., 2015. Hydrologic connectivity constrains partitioning of global terrestrial water fluxes. Science 349 (6244), 175–177.

Jasechko, S., Sharp, Z.D., Gibson, J.J., Birks, S.J., Yi, Y., Fawcett, P.J., 2014. Jasechko et al. reply. Nature 506 (7487), E2–E3.

Jefferson, J.L., Maxwell, R.M., 2015. Evaluation of simple to complex parameterizations of bare ground evaporation. J. Adv. Model. Earth Syst. 7 (3), 1075–1092.

Katul, G.G., Oren, R., Manzoni, S., Higgins, C., Parlange, M.B., 2012. Evapotranspiration: a process driving mass transport and energy exchange in

the soil-plant-atmosphere-climate system. Rev. Geophys. 50, RG3002. https://doi.org/10.1029/2011RG000366.
Kollet, S.J., Maxwell, R.M., 2006. Integrated surface–groundwater flow modeling: a free-surface overland flow boundary condition in a parallel groundwater flow model. Adv. Water Resour. 29, 945–958.
Kuo, W.L., Steenhuis, T.S., McCulloch, C.E., Mohler, C.L., Weinstein, D.A., DeGloria, S. D., Swaney, D.P., 1999. Effect of grid size on runoff and soil moisture for a variable-source-area hydrology model. Water Resour. Res. 35 (11), 3419–3428.
Lawrence, D.M., Thornton, P.E., Oleson, K.W., Bonan, G.B., 2007. The partitioning of evapotranspiration into transpiration, soil evaporation, and canopy evaporation in a GCM: impacts on land–atmosphere interaction. J. Hydrometeorol. 8 (4), 862–880.
Lawrence, P.J. et al., 2012. Simulating the biogeochemical and biogeophysical impacts of transient land cover change and wood harvest in the community climate system model (CCSM4) from 1850 to 2100. J. Clim. 25 (9), 3071–3095. https://doi.org/10.1175/JCLI-D-11-00256.1.
Li, L., van der Tol, C., Chen, X., Jing, C., Su, B., Luo, G., Tian, X., 2013. Representing the root water uptake process in the Common Land Model for better simulating the energy and water vapour fluxes in a Central Asian desert ecosystem. J. Hydrol. 502, 145–155.
Maxwell, R.M., 2013. A terrain-following grid transform and preconditioner for parallel, large-scale, integrated hydrologic modeling. Adv. Water Resour. 53, 109–117.
Maxwell, R.M., Condon, L.E., 2016. Connections between groundwater flow and transpiration partitioning. Science 353 (6297), 377–380.
Miralles, D.G., De Jeu, R.A., Gash, J.H., Holmes, T.R., Dolman, A.J., 2011. Magnitude and variability of land evaporation and its components at the global scale. Hydrol. Earth Syst. Sci. 15, 967–981.
Oleson, K.W., Niu, G.Y., Yang, Z.L., Lawrence, D.M., Thornton, P.E., Lawrence, P.J., Stockli, R., Dickinson, R.E., Bonan, G.B., Levis, S., Dai, A., Qian, T., 2008. Improvements to the Community Land Model and their impact on the hydrological cycle. J. Geophys. Res. 113. https://doi.org/10.1029/2007JG000563.
Sellers, P.J., Randall, D.A., Collatz, G.J., Berry, J.A., Field, C.B., Dazlich, D.A., Zhang, C., Collelo, G.D., Bounoua, L., 1996. A revised land surface parameterization (SiB2) for atmospheric GCMs: Part I. Model formulation. J. Clim. 9 (4), 676–705.
Schlesinger, W.H., Jasechko, S., 2014. Transpiration in the global water cycle. Agric. For. Meteorol. 189–190, 115–117.
Shrestha, P., Sulis, M., Masbou, M., Kollet, S., Simmer, C., 2014. A scale-consistent Terrestrial System Modeling Platform based on COSMO, CLM and ParFlow. Mon. Wea. Rev. 142, 3466–3483. https://doi.org/10.1175/MWR-D-14-00029.1.
Shrestha, P., Sulis, M., Simmer, C., Kollet, S., 2015. Impacts of grid resolution on surface energy fluxes simulated with an integrated surface-groundwater flow model. Hydrol. Earth Syst. Sci. 19 (10), 4317–4326.
Sulis, M., Langensiepen, M., Shrestha, P., Schickling, A., Simmer, C., Kollet, S.J., 2015. Evaluating the influence of plant-specific physiological parameterizations on the partitioning of land surface energy fluxes. J. Hydrometeorol. https://doi.org/10.1175/JHM-D-14-0153.1.
Sulis, M., Paniconi, C., Camporese, M., 2011. Impact of grid resolution on the integrated and distributed response of a coupled surface–subsurface hydrological model for the des Anglais catchment, Quebec. Hydrol. Process. 25 (12), 1853–1865.
Tang, J., Riley, W.J., 2013. Impacts of a new bare-soil evaporation formulation on site, regional, and global surface energy and water budgets in CLM4. J. Adv. Model. Earth Syst. 5, 558–571. https://doi.org/10.1002/jame.20034.
Waldhoff, G., 2012. Enhanced Land Use Classification of 2009 for the Rur catchment. CRC/TR32 Database (TR32DB), http://dx.doi.org/10.5880/TR32DB.2.
Wang, Y., Xie, Z., Jia, B., 2016. Incorporation of a dynamic root distribution into CLM4: 5. Evaluation of carbon and water fluxes over the Amazon. Adv. Atmos. Sci.9 33, 1047–1060.
Zhang, Y.Q., Peña-Arancibia, J.L., McVicar, T.R., Chiew, F.H.S., Vaze, J., Liu, C.M., Lu, X.J., Zheng, H.X., Wang, Y.P., Liu, Y.Y., Miralles, D.G., Pan, M., 2016. Multi-decadal trends in global terrestrial evapotranspiration and its components. Sci. Rep. 6, 19124. https://doi.org/10.1038/srep19124.
Zeng, X., Dai, Y.-J., Dickinson, R.E., Shaikh, M., 1998. The role of root distribution for land climate simulation. Geophys. Res. Lett. 25, 4533–4536.
Zhang, W., Montgomery, D.R., 1994. Digital elevation model grid size, landscape representation, and hydrologic simulations. Water resour. res. 30 (4), 1019–1028.